Dynamic contact angle measurements on superhydrophobic surfaces

Jeong-Hyun Kim, H. Pirouz Kavehpour, and Jonathan P. Rothstein

Citation: Physics of Fluids (1994-present) **27**, 032107 (2015); doi: 10.1063/1.4915112
View online: http://dx.doi.org/10.1063/1.4915112
View Table of Contents: http://scitation.aip.org/content/aip/journal/pof2/27/3?ver=pdfcov
Published by the AIP Publishing

PHYSICS OF FLUIDS **27**, 032107 (2015)

Dynamic contact angle measurements on superhydrophobic surfaces

Jeong-Hyun Kim,[1] H. Pirouz Kavehpour,[2] and Jonathan P. Rothstein[1,a)]
[1]*Department of Mechanical and Industrial Engineering, University of Massachusetts Amherst, 160 Governors Drive, Amherst, Massachusetts 01003-2210, USA*
[2]*Department of Mechanical and Aerospace Engineering, University of California, Los Angeles, California 90095-1597, USA*

(Received 17 September 2014; accepted 3 March 2015; published online 19 March 2015; corrected 25 March 2015)

In this paper, the dynamic advancing and receding contact angles of a series of aqueous solutions were measured on a number of hydrophobic and superhydrophobic surfaces using a modified Wilhelmy plate technique. Superhydrophobic surfaces are hydrophobic surfaces with micron or nanometer sized surface roughness. These surfaces have very large static advancing contact angles and little static contact angle hysteresis. In this study, the dynamic advancing and dynamic receding contact angles on superhydrophobic surfaces were measured as a function of plate velocity and capillary number. The dynamic contact angles measured on a smooth hydrophobic Teflon surface were found to obey the scaling with capillary number predicted by the Cox-Voinov-Tanner law, $\theta_D{}^3 \propto Ca$. The response of the dynamic contact angle on the superhydrophobic surfaces, however, did not follow the same scaling law. The advancing contact angle was found to remain constant at $\theta_A = 160°$, independent of capillary number. The dynamic receding contact angle measurements on superhydrophobic surfaces were found to decrease with increasing capillary number; however, the presence of slip on the superhydrophobic surface was found to result in a shift in the onset of dynamic contact angle variation to larger capillary numbers. In addition, a much weaker dependence of the dynamic contact angle on capillary number was observed for some of the superhydrophobic surfaces tested. [http://dx.doi.org/10.1063/1.4915112]

INTRODUCTION

Superhydrophobic surfaces have been observed in many plants and insects around the world.[1–7] They are characterized by two important factors: chemical hydrophobicity and micron or nanometer sized surface roughness. The combination of low surface energy and surface roughness can trap an air layer on the surface, resulting in the formation of air-water interface between the peaks of surface roughness. The presence of the air-water interface can result in a large static advancing contact angle, $\theta_A > 150°$, and little contact angle hysteresis which is defined as the difference between advancing and receding contact angles, $\theta_A \approx \theta_R$. This extreme water repellency gives the lotus leaf and other plants their self-cleaning properties, allows water strider to walk or even jump on the water,[3] and makes it possible for insects and spiders to breath under water.[2,5] The low contact angle hysteresis also enables droplets to move easily across the surface due to the reduction of the pinning force.[8–11] In addition, superhydrophobic surfaces have been shown to reduce drag in both laminar and turbulent flow. The presence of air-water interface changes the boundary condition on the superhydrophobic surfaces from the classic no-slip condition to a partial slip condition.[12–15]

In the superhydrophobic surface literature, only static advancing and receding contact angles have been reported to date. However, under flow conditions, the dynamics of the three phase contact line and the resulting dynamic contact angles are known to be influenced by molecular-level adsorption/

a)e-mail: rothstein@engin.umass.edu

desorption phenomena and macroscopic flow-induced viscous dissipation.[16,17] Dynamic contact angle measurements have been made for a wide variety of different liquids and surfaces,[17–19] yet no dynamic contact angle measurements exist for superhydrophobic surfaces. From the measurements in the literature and the predictions of theoretical calculations, the dynamic advancing contact angle has been shown to increase with increasing velocity of the three phase contact line, while the dynamic receding contact angle has been found to decrease with increasing velocity. If we are to fully understand the motion of droplets, jets, and streams along superhydrophobic surfaces, it is essential that measurements of the dynamic contact angle on superhydrophobic surfaces be performed.

Several techniques have been introduced to measure the dynamic contact angles. For the case of forced wetting, displacement of liquid in a capillary tube and plunging a surface into a tank are common techniques to measure the dynamic contact angles. In both experiments, the gravity and inertial effects can typically be neglected. The early experiments of Hoffman used a glass capillary tube and measured the variation of dynamic contact angles over a wide range of wetting velocities.[18] By normalizing the data with the capillary numbers, $Ca = \mu U/\gamma$, where μ is the viscosity, U is the spreading velocity, and γ is the interfacial tension, Hoffman showed that all the dynamic contact angle data could be collapsed onto a single master curve.[18] The plunge tank configuration is frequently used to measure the dynamic contact angle because it provides easy access to visualize the contact line. In this experiment, the contact line is observed as the solid substrate, typically a Wilhelmy plate or a cylindrical strand of material, is immersed into an open container of liquid.[20–23] Petrov *et al*. showed that one advantage of the plunge-tank technique is the ability to probe both the dynamic advancing and receding contact angles and as a result the dynamic contact angle hysteresis.[24]

In order to understand the origins of the dynamic contact angle, one must consider the macroscopic and molecular dynamics occurring in close proximity to the three phase contact line. If, as is conventional in continuum fluid dynamics, the no-slip boundary condition is assumed, the viscous stress in the fluid and the force applied to the solid become infinite at a moving three phase contact line.[25] This stress singularity makes solution of the Navier-Stokes equations impossible with a moving contact line. By relaxing the no-slip condition at the contact line and allowing for a small but finite slip, Voinov[26] derived a hydrodynamic relation between the contact line speed and the contact angle of liquids as they spread across a solid surface. Voinov[26] assumed capillary number was small ($Ca << 1$) and that the liquid-gas interface could be considered static far from the contact line. The contact angle of the drops was also assumed to be sufficiently small to allow for a lubrication analysis to be used which amongst other things allow the motion of the liquid in the drops to be treated as one-dimensional. These assumptions lead to the classic relationship between dynamic contact angle and the capillary number, $\theta_D{}^3 \propto Ca$. The same scaling was derived for the spreading of a fully wetting drop by Tanner.[27] This result is known as the Cox-Voinov-Tanner scaling law. By matching the static or equilibrium contact angle with the hydrodynamic solution, Voinov[26] and later Cox[28] were able to obtain an exact solution for partially wetting fluids which we will call the Cox-Voinov model,

$$\theta_D{}^3 = \theta_S{}^3 \pm (9\mu U/\gamma)\ln(L/b). \tag{1}$$

Here, θ_S is static contact angle, L is characteristic length scale of the outer region of the flow, and b is the slip length. For most surfaces, the slip length is on the order of $b \approx 10^{-9}$ m or less. Often the outer length scale is chosen to be a constant times the capillary length, $L = \alpha\,\kappa^{-1} = \alpha\sqrt{\gamma/\rho g}$. The value of the constant α is not universal and has been shown to be dependent on the flow geometry as well as the boundary conditions.[26,29–31] Perhaps most interesting, the predictions of Eggers and Stone[30] showed that α may not even be a constant at all but instead dependent on the capillary number of the flow. It is also important to note that the value of the constant, α, depends on whether the contact line is advancing or receding.[29] Eggers[32] predicted that the form of Eq. (1) holds for the dynamic receding contact angle; however, the value of the constant is different than that found by Hocking[31] for dynamic advancing contact and is given by $\alpha = 2\left(\cos\theta_{plate} - \cos\theta_S\right)/3$. Here, θ_{plate} is the plunge angle the plate makes with the horizontal. It is this form that we will use to fit our receding contact angle data.

At low to moderate capillary numbers, the dynamic contact angle measurements on liquid/solid systems with complete and partial equilibrium wetting have been found to follow the Cox-Voinov-Tanner scaling law over a wide range of flow configurations.[18,21,33,34] Surprisingly, the Cox-Voinov

model given in Eq. (1) has been shown to hold even at large contact angles. In these cases of partially wetting fluids, Snoeijer[35] showed that the solution to the hydrodynamic model for droplet spreading can be generalized beyond the assumptions of the small contact angle and lubrication flow and did not deviate by more than a few percent from Eq. (1) up to angles as large as 150°. Although it is widely accepted, the Cox-Voinov-Tanner scaling law is not universal. It has been observed to fail at extremely low capillary number regime, $Ca < 10^{-4}$, and at very large capillary numbers, $Ca > O(0.1)$, where air entrainment, complete coating, and the effects of inertia have been observed.[36] In addition to the hydrodynamic models, a number of other physical and empirical models exist to describe the evolution of the dynamic contact angle with capillary number.[36,37]

Blake and Haynes developed a molecular kinetic theory in order to explain the motion of three phase contact line and the dynamic contact angle.[38] In this approach, the dependence of the dynamic contact angle on the contact line velocity is the result of molecular adsorption and desorption at the moving contact line. The dynamic contact angle is related to velocity by

$$\theta_D = \cos^{-1}[\cos\theta_S - (2k_BT/\gamma\lambda^2)\sinh^{-1}(U/2K_\omega\lambda)], \tag{2}$$

where k_B is the Boltzmann constant and T is the temperature. The constant λ relates to the distance between adsorption sites on the solid surface and the constant K_ω is the equilibrium frequency of the random molecular displacements occurring within the three-phase zone. These parameters are determined by a curve fitting of experimental data and typically have approximately 10^{-9} m and 10^6 s^{-1}. In many cases, especially at low velocities, the molecular-kinetic model fits the experimental data well.[39–41] Unfortunately, there is no definitive way of predicting the values of the parameters K_ω and λ *a priori*.

There have been a large number of experimental results predicted by each wetting theory despite their fundamentally different physics and approaches. For small dynamic contact angles, the hydrodynamic and molecular kinetic models predict fundamentally different scaling laws such that $\theta_D{}^3 \propto U$ and $\theta_D{}^2 \propto U$, respectively. The applicability of these two theories has been debated in the literature. However, it is clear that both the viscous dissipation and the wetting-line friction play a role in determining the dynamic contact angle.

In this paper, we will present the first dynamic contact angle measurements on superhydrophobic surfaces. Two different superhydrophobic surfaces, one randomly rough and one precisely patterned, will be fabricated and tested with a series of different aqueous solution with different viscosities so that the dynamic contact angle can be measured over a large range of capillary numbers. The experimental results presented in this paper will demonstrate that the dynamic wetting on superhydrophobic surfaces does not follow the scaling law predicted by either the hydrodynamic or the molecular kinetic model. Instead, we will show that for superhydrophobic surfaces, the dynamic contact angle has a much weaker dependence on contact line speed.

DESCRIPTION OF THE EXPERIMENT

A modified Wilhelmy plate method was used to measure the dynamic advancing and receding contact angles. A schematic diagram of the Wilhelmy plate is presented in Figure 1. In this study, both hydrophobic and superhydrophobic plates were used. The hydrophobic surface was fabricated from a smooth PTFE (Teflon) sheet purchased from McMaster-Carr which has a RMS roughness measured to be 5 μm.[42] The static contact angles on the smooth PTFE were measured to be $\theta_{A,s} = 98°$ and $\theta_{R,s} = 81°$, respectively.

Two different superhydrophobic surfaces were also studied: one having randomly distributed surface roughness and the other containing a regular pattern of surface roughness. The randomly rough surface consisted of an acrylic plate spray painted with a commercially available superhydrophobic paint (WX2100, Cytonix). A SEM image of the surface is presented in Figure 2 to show the details of the resulting surface topography. The paint consists of particles approximately 5 μm in diameter suspended in a hydrophobic fluorothane resin. Upon deposition, a surface with random granular features was produced as seen in Figure 2. The RMS roughness of the final surfaces was on the same order as the particle size. The static advancing and receding contact angles on the spray-painted surface were measured to be $\theta_{A,s} = 159°$ and $\theta_{R,s} = 140°$.

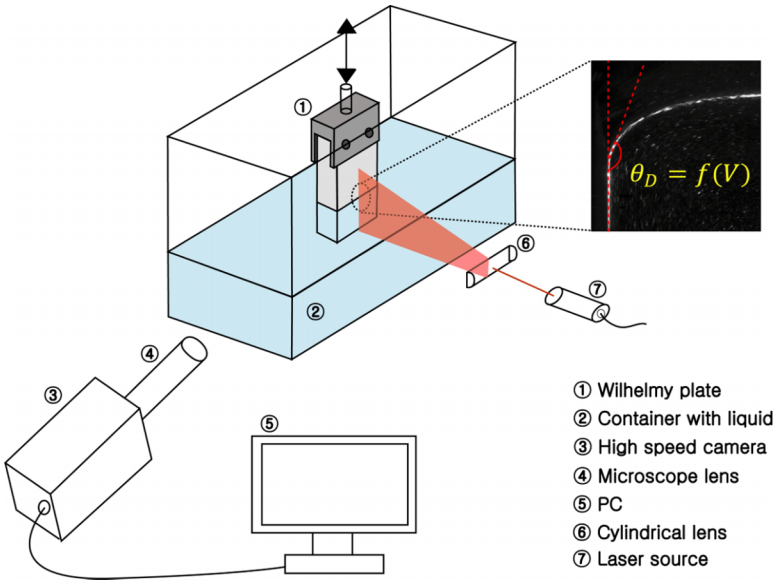

FIG. 1. Schematic diagram showing the modified Wilhelmy plate method used in these experiments.

The regularly patterned superhydrophobic surface was fabricated by hot embossing a pattern of posts into a smooth PTFE surface. A woven stainless steel mesh with 38 μm diameter wires spaced 38 μm apart was used as the master and a hot press raised to 325 °C was used to drive the PTFE into the spaces between the wire mesh. A microscope image of the resulting surface topography can be seen in Figure 3. The patterned PTFE surface contains a series of elongated oval-shaped posts, measured to be roughly 40 μm wide, 80 μm long, and 40 μm tall. Due to the weave of the stainless steel mesh, the orientation of adjacent posts can be seen in Figure 3 to be rotated by 90° with respect to each other. The minimum spacing between posts is roughly 40 μm. The static advancing and receding contact angles on the superhydrophobic PTFE surface were measured to be $\theta_{A,s} = 151°$ and $\theta_{R,s} = 144°$.

A series of test fluids were used with different viscosities so that the capillary number could be systematically varied. The initial test fluid was water. In addition, a series of high viscosity aqueous solutions were used. The first solution consisted of 20 wt. % of a low molecular weight polyethylene oxide (PEO) (Mw = 20 000 g/mol) in water. The second solution was 83% glycerin in water. Both solutions were gently mixed for at least 24 h to ensure complete dissolution. Both the aqueous PEO and glycerin in water solutions had a constant viscosity of $\mu = 0.063$ Pa s and surface tensions of $\gamma = 60$ mN/m.

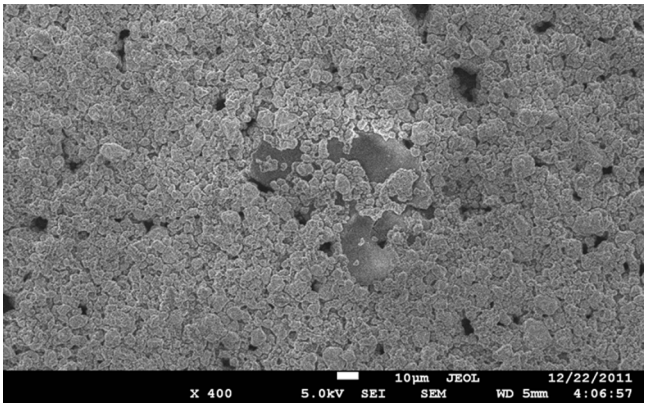

FIG. 2. A SEM image of a superhydrophobic paint surface.

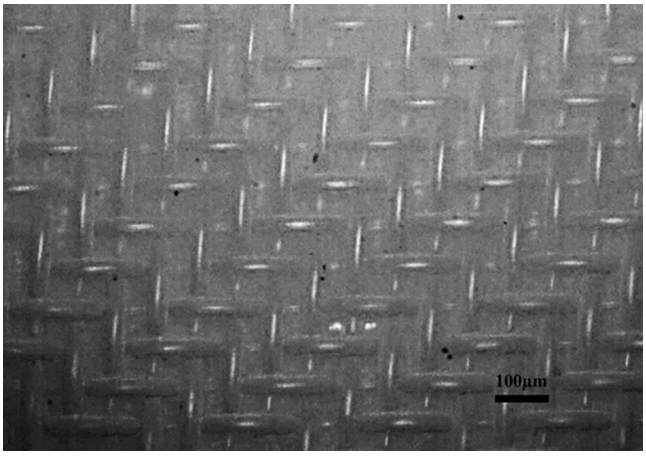

FIG. 3. A microscope image of the surface structure for a superhydrophobic PTFE surface.

The test surfaces were attached to a linear motor and were alternately immersed into and withdrawn from a reservoir of the test fluid so that the advancing and receding contact angles could be measured. No significant change in the dynamic contact angle measurements was observed with multiple sequential immersions of the plate into the reservoir. Additionally, the plate was found to be dry to the touch upon removal from the fluid. The curvature of the air-liquid interface near the contact line was recorded by a high-speed camera at sample rates up to 200 Hz and optically zoomed in so that a 3 cm × 3 cm field of view could be observed. To effectively visualize the flow, 13 μm diameter silvered hollow glass spheres (Sphericel, Potters Industry), often used for particle image velocimetry (PIV), were added to the test fluids at concentrations less than 0.1 wt. %. The particles were not surface active, and as a result, they were not observed to populate the air-liquid interface or to come out of solution and deposit on the Wilhelmy plate. Additionally, these particles have been used in previous studies to visualize flow past superhydrophobic surfaces and have not been observed to affect the flow or adsorb to the air water interface trapped along the superhydrophobic surface.[13,43] A 5 mW diode laser and a cylindrical lens were used to generate a laser light sheet and illuminate a plane in the fluid in order to visualize the deformation of the interface. The solid substrate was accelerated from rest to a constant velocity between $2\ \text{mm/s} < U < 200\ \text{mm/s}$, which corresponds to capillary number range between $10^{-5} < Ca < 0.3$ depending on fluid properties.

The dynamic contact angles were determined by analyzing the high-speed video images as seen in Figure 1 using the program ImageJ. The angles were measured manually by first digitally zooming into the image by a factor of five and then fitting a line through roughly the first 500 μm of the interface. Multiple measurements at each flow condition were taken and a statistical analysis performed. For the smooth PTFE surfaces, the uncertainty of the averaged experimental measurements was ±1°. While for the superhydrophobic surfaces, the uncertainty was found to be a little larger at ±3° due to the added noise associated with the unsteadiness of the contact line moving along a rough, partially wetting surface.

The sensitivity of the measurements to the spatial resolution of the images was studied by varying the optical/digital magnification of the contact line by an order of magnitude and making multiple measurements of the contact angle. No discernible trend in the data was observed with increasing resolution, but a standard deviation in the data at different magnifications of around 1° was found for both the hydrophobic and the superhydrophobic surfaces. Note that the images with the maximum spatial resolution of these experiments contained 30 μm square pixels. To ensure steady-state was reached in each case, the contact angle measurements were always performed at the mid-point of the substrates. This also aided with measurement consistency especially for the case of the superhydrophobic surface where variation in surface roughness and wettability across the substrate were found to affect the contact angle measurements by as much as 6°.

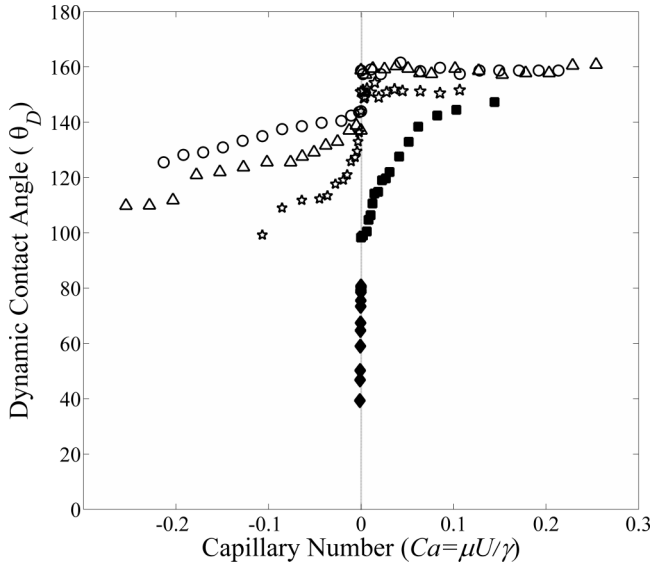

FIG. 4. Dynamic contact angle as a function of capillary number. The data include the superhydrophobic paint surface with (circle) glycerin solution and (triangle) PEO solution, (star) the superhydrophobic PTFE surface with glycerin solution, a smooth PTFE surface with (closed square) PEO solution and (closed diamond) pure water. The smooth PTFE data have an uncertainty of ±1°, while the superhydrophobic data have an uncertainty of ±3°.

RESULTS AND DISCUSSION

In Figure 4, the variations of both advancing and receding contact angles are plotted as a function of the capillary number for both the hydrophobic and superhydrophobic surfaces. The advancing contact angles are all plotted against a positive capillary number while the receding contact angles are plotted against a negative capillary number to differentiate the two regimes. To avoid confusion in an already busy figure, the error bars are not superimposed over the data but the value of the uncertainty is quoted in the caption. The dynamic contact angle measurements on the smooth PTFE surface showed a monotonic increase/decrease in the advancing/receding contact angle with increasing substrate velocity. At large capillary numbers, the advancing contact angle was found to approach an asymptotic value of $\theta_A = 150°$. This is consistent with measurements in the literature.[18]

For these superhydrophobic surfaces, the first deviation from the expected dynamic contact angle behavior that was observed occurred for the advancing contact angle measurements. Within experimental error, the advancing contact angles measured for these superhydrophobic surfaces were found to be insensitive to changes in the velocity of the solid substrate. This was true even at the very highest capillary numbers tested, $Ca \sim 0.2$. From this observation, it is clear that neither the hydrodynamic models nor the molecular theory can describe the advancing contact angles on superhydrophobic surfaces. These measurements, instead, suggest that for superhydrophobic surfaces; the advancing contact angle is independent of contact line velocity.

As seen in Figure 4, the receding contact angle was found to decrease monotonically with increasing capillary number for all the surfaces and fluids tested. On this linear scale, the variation in receding contact angle of the smooth PTFE surface appears very steep and was confined to the low capillary number regime. On the logarithmic scale used in subsequent plots, these data will be expanded and the scaling compared to both hydrodynamic and molecular models of dynamic contact angle. One interesting observation is that the decay in the receding contact angle with increasing capillary number for the superhydrophobic surfaces was significantly slower than for the smooth hydrophobic PTFE surfaces. As a result, due to the limitations of the velocity of the Wilhelmy plate, very little contact angle variation was achieved using water because the accessible capillary numbers were too small. In order to access a higher capillary number range, the glycerin in water and PEO in water test fluids were used because they have significantly higher viscosities than water. The delay in the onset of dynamic contact angle variation and the reduction in the magnitude of variation are likely the result of

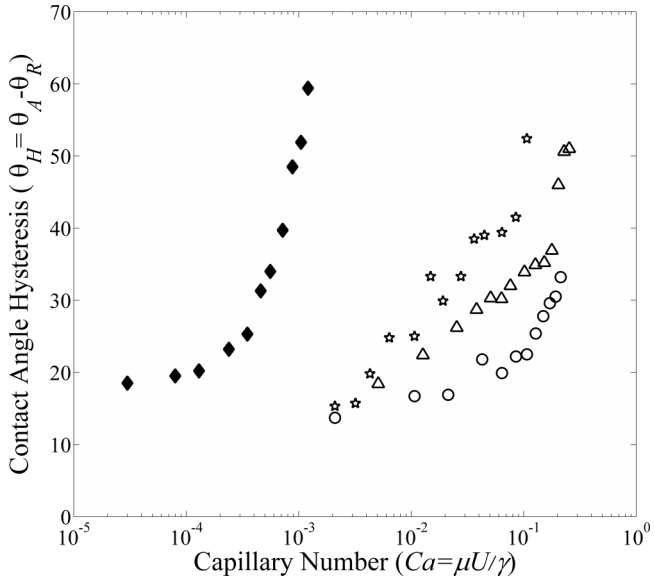

FIG. 5. Contact angle hysteresis as a function of capillary number. The data include the superhydrophobic paint surface with (circle) glycerin solution and (triangle) PEO solution, (star) the superhydrophobic PTFE surface with glycerin solution, a smooth PTFE surface with (closed diamond) pure water. The smooth PTFE data have an uncertainty of ±1°, while the superhydrophobic data have an uncertainty of ±3°.

the reduction in viscous stress due to the presence of the shear-free air-liquid interface trapped within the features of the superhydrophobic surface. Superhydrophobic surfaces are known to produce slip at the wall which can easily result in slip lengths of more than 10 μm.[44] Even though this slip length is small in comparison to the macroscopic length scales of this flow, a slip length of 10 μm can still result in a significant reduction in the viscous stress, especially in the region of the flow close to the three phase contact line where the shear rate diverges if the no-slip boundary condition is imposed.

The effect of reduction in the viscous stress on superhydrophobic surfaces is apparent in the variations of the contact angle hysteresis. The contact angle hysteresis was calculated from the difference between dynamic advancing and receding contact angles and plotted with capillary numbers as shown in Figure 5. The fast decay of the dynamic receding contact angles for the smooth PTFE surface led to a dramatic increase in contact angle hysteresis in the low capillary number regime. For superhydrophobic surfaces, the introduction of regularly patterned or random features and the shear-free interface supported between them can induce a partial-slip boundary condition on the surface. As a result, the onset of changes to the contact angle hysteresis of superhydrophobic surfaces was found to be significantly delayed with the onset moving from $Ca = 10^{-4}$ to $Ca = 10^{-3}$ or even higher depending on the superhydrophobic surface tested.

To investigate the scaling trends of receding contact angles and to compare to the predictions of the hydrodynamic model in Eq. (1), the difference between the cube of the static and dynamic receding contact angles was calculated and plotted against capillary number in Figure 6. The static contact angle of each data set was determined by extrapolation to zero capillary number using a cubic polynomial to fit between five and ten of the lowest capillary number data points. As seen in Figure 6, the receding contact angle data for pure water receding along the hydrophobic PTFE surface were found to scale like $\theta_{R,s}{}^3 - \theta_R{}^3 \propto Ca$ as predicted by the hydrodynamic Cox-Voinov-Tanner scaling law as shown by the fit superimposed over the data in Figure 6. Note that although it is not shown in Figure 6, the advancing contact angle data for smooth PTFE were also found to follow the Cox-Voinov-Tanner scaling law.

In contrast to the smooth PTFE surface, the behavior of the receding contact angle on the superhydrophobic surfaces was found to be more complex. None of the superhydrophobic surfaces tested were well fit over their entire range by the Cox-Voinov-Tanner scaling law. First, we will consider the superhydrophobic painted surfaces. At low to moderate capillary numbers, $Ca < 10^{-2}$, both the PEO

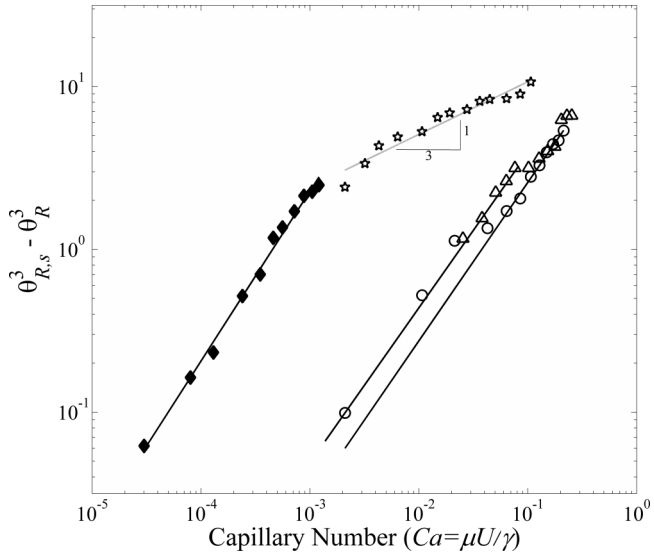

FIG. 6. Plot of the difference in the cube of the static receding contact angle and the cube of the dynamic receding contact angle as a function of capillary number. The data include the superhydrophobic paint surface with (circle) glycerin solution and (triangle) PEO solution, (star) the superhydrophobic PTFE surface with glycerin solution, a smooth PTFE surface with (closed diamond) pure water. The smooth PTFE data have an uncertainty of ±1°, while the superhydrophobic data have an uncertainty of ±3°. The solid lines represent fits to the Cox-Voinov-Tanner law with different slip lengths. For the superhydrophobic paint surface at low capillary numbers, both data sets are fit well by a slip length of $b = 12$ μm, while at large capillary numbers, the data are fit by a slip length of $b = 78$ μm.

and glycerin in water solutions appear to follow the Cox-Voinov-Tanner scaling law. Using Eq. (1), with $\alpha = 2\left(\cos\theta_{plate} - \cos\theta_{R,s}\right)/3$ as shown by Eggers,[32] it is possible to fit the experimental data in this region and infer a value of the slip length. In this moderate capillary number region, a value of $b = 12$ μm in Eq. (1) fits both data sets very well. This value of slip length compares well to the direct laminar flow measurements of the slip length for the spray-painted superhydrophobic surfaces that we made using the experimental procedure outlined in Song *et al.*[44] In those microfluidics experiments, a value of $b = 10$ μm was found for the superhydrophobic painted surface and a value of $b = 6$ μm was found for the superhydrophobic PTFE surface.

At a critical capillary number, a transition to a much weaker capillary number dependence in receding contact angle, ${\theta_{R,s}}^3 - {\theta_R}^3 \propto Ca^n$, where $n < 1$, was observed in both cases. For the superhydrophobic painted surface with the glycerin in water solution, the transition was found to occur at a capillary number of $Ca_{crit} \approx 0.02$ while for the PEO in water solution the transition did not occur until a capillary number of $Ca_{crit} \approx 0.08$. In each case, a slope close to $n = 1/2$, or ${\theta_{R,s}}^3 - {\theta_R}^3 \propto Ca^{1/2}$, was observed. Interestingly, beyond a capillary number of $Ca > 0.1$, the data for both fluids on the superhydrophobic paint surface transition back to a slope of one and the predictions of Cox-Voinov model but with a much larger slip length of $b = 78$ μm. The physical origin of this transition at high capillary number to a larger apparent slip length is not obvious. One possibility is that the increased slip length might be evidence of dynamic dewetting from some of the features of the randomly rough spray-painted superhydrophobic surface.

For the case of the superhydrophobic PTFE surface, no region consistent with the Cox-Voinov-Tanner scaling law was observed. Instead, the data were found to have a consistent slope of ${\theta_{R,s}}^3 - {\theta_R}^3 \propto Ca^{1/3\pm0.08}$ or $({\theta_{R,s}}^3 - {\theta_R}^3)^3 \propto Ca$ over more than two decades of capillary number. Note that the uncertainty reported in the slope is due to the ±3° uncertainty in the contact angle measurements. This scaling is also inconsistent with the predictions of the Blake and Haynes[38] molecular kinetics model for which a scaling of ${\theta_{R,s}}^2 - {\theta_R}^2 \propto Ca$ is expected for small capillary numbers. Additionally, this scaling is inconsistent with the effects of inertia for which a scaling of ${\theta_{R,s}}^3 - {\theta_R}^3 \propto Ca^2$ would likely be observed. Each of these theories predicts a dependence of the contact angle on the capillary number of between $\theta_R \propto Ca^{1/2}$ and $\theta_R \propto Ca^{2/3}$ while the data clearly show a much weaker dependence of $\theta_R \propto Ca^{1/9}$.

For the superhydrophobic surfaces, both the hydrodynamic and molecular-kinetic models were able to partially fit the experimental data. However, neither of the two conventional models describes the weak dependence on capillary number observed for the superhydrophobic PTFE surface or the transitions observed for the superhydrophobic paint surfaces at moderate capillary numbers. In order to demonstrate the dependence of dynamic contact angles on the velocity over the entire velocity range, a combined model proposed by Petrov and Petrov[45] was tested. In this model, it is assumed that the static contact angle in the Cox-Voinov hydrodynamic model in Eq. (1) is velocity dependent and that an appropriate value for the static contact angle can be obtained from Blake and Haynes' molecular-kinetic equation as shown in Eqs. (3) and (4),

$$\theta_D{}^3 = [\theta_S(U)]^3 \pm (9\mu U/\gamma)\ln(L/b), \tag{3}$$

$$\theta_S(U) = \cos^{-1}[\cos\theta_{S,0} \mp (2k_BT/\gamma\lambda^2)\sinh^{-1}(U/2K_\omega\lambda)]. \tag{4}$$

Here, $\theta_S(U)$ is velocity dependent static contact angle and $\theta_{S,0}$ is the static contact angle at rest. It was found to be capable of fitting the experimental data over its entire range as seen in Figure 7. Unfortunately, although the model did fit the data, a physical interpretation of the variation in the model fit parameters could not be inferred from the data. For each case, best fit to the distance of molecular displacement, λ, was of the same order of molecular length, $\lambda \sim 10^{-9}$ m. However, for glycerin and polyethylene solutions on same superhydrophobic paint surface, the frequency of adsorption and desorption, K_ω, differed by a factor of about 100. This result implies that the selection of the testing fluid can make different behaviors of dynamic contact angles with capillary number even if each solution has same viscosity and surface tension and was tested on the same superhydrophobic surface. In each case, the slip length used in the combined model was fixed at $b_{SHS} = 78$ μm. However, it should be noted that equally good fits could be achieved with Petrov's combined model for slip lengths that were unphysical and as large as $b = 250$ μm. The success of the combined model in capturing the trends in the data suggests that the role of the molecular stress is important for the case of superhydrophobic surfaces and can influence the dynamic contact angle measurements even at relatively large capillary numbers due to the dramatic reduction of the viscous stress resulting from slip.

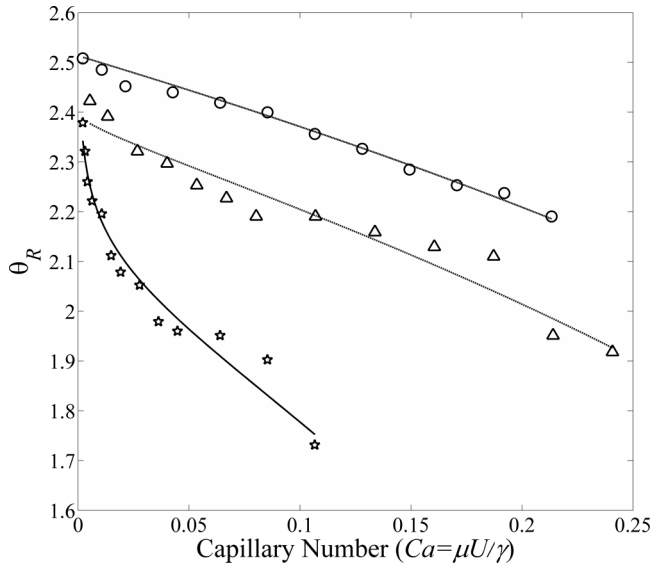

FIG. 7. Fitting of the combined model to the receding contact angle as a function of capillary number. The data include superhydrophobic paint surface with (circle) glycerin solution and (triangle) PEO solution, (star) a superhydrophobic PTFE surface with glycerin solution. The superhydrophobic data have an uncertainty of ±3°. The parameters used are below. For superhydrophobic paint surface with (circle) glycerin solution, $\lambda = 7.3$ nm, $K_\omega = 3.4\times10^7$, $b = 78$ μm. For superhydrophobic paint surface with (triangle) PEO solution, $\lambda = 4.7$ nm, $K_\omega = 5.5\times10^5$, $b = 78$ μm. For a superhydrophobic PTFE surface with glycerin solution, $\lambda = 1.41$ nm, $K_\omega = 3.1\times10^5$, $b = 78$ μm.

Finally, we should note that at the largest capillary numbers reached in these experiments, a transition is often observed from continuous dewetting of the fluid to the deposition of a smooth uniform Landau-Levich film.[29] However, no film was deposited in any of the experiments presented here. All the surfaces were found to be dry upon removal from the liquid bath; although, there has been work that has shown that a very small amount of fluid can be pinched off and remain behind on the top of the features of a superhydrophobic surface as the interface recedes.[46] This is further evidence that the large slip lengths of these superhydrophobic surfaces can dramatically reduce the viscous stresses developed near the contact line which de Gennes[47] showed were responsible for the dynamic wetting transition to film coating at large capillary numbers.

SUMMARY

In this paper, we have performed a series of dynamic contact angle measurements by using a modified Wilhelmy plate method with hydrophobic and superhydrophobic surfaces. The water and aqueous solutions of polyethylene oxide solutions and glycerin solutions were studied in order to vary the liquid's viscosity. The hydrophobic smooth PTFE surface showed significant asymmetry in the dynamic contact angles with respect to the capillary number. However, both the advancing and receding angles were found to follow the hydrodynamic Cox-Voinov-Tanner scaling law, i.e., $\theta_{R,s}{}^3 - \theta_R{}^3 \propto Ca$. The dynamic contact angles measured for the superhydrophobic surfaces showed very different characteristics. The presence of microscale structures on the surface of a regularly patterned superhydrophobic PTFE surface and a randomly rough superhydrophobic spray-painted surface resulted in large static advancing and receding contact angles and little static contact angle hysteresis. For all of the superhydrophobic surfaces tested, the advancing contact angles were found to be independent of the capillary number even as the capillary number was driven in excess of $Ca > 0.1$. This observation is a direct result of the reduction of viscous stress at the three-phase contact line caused by from the presence of slip along the superhydrophobic surface. The reduction of viscous stress was also found to have a large impact on the dynamic receding contact angles measured for each of the superhydrophobic surfaces. For the superhydrophobic PTFE surface, the receding contact angle was found to decrease with increasing capillary number, but at a rate that was much weaker than that predicted by the hydrodynamic Cox-Voinov-Tanner scaling law or the Blake-Haynes molecular kinetic theory, $\theta_{R,s}{}^3 - \theta_R{}^3 \propto Ca^{1/3}$. For superhydrophobic spray-painted surfaces, however, a different behavior was observed. For those surfaces, the dynamic receding contact angles were described well at low capillary numbers by the Cox-Voinov model with a slip length of approximately $b = 12\ \mu$m. This slip length closely matches the value independently measured for these surfaces in microfluidic drag reduction experiments. At moderate capillary numbers, a transition to a weaker capillary number dependence was observed similar to the case for the superhydrophobic PTFE surface. Finally, at larger capillary numbers, the data were again found to follow the Cox-Voinov-Tanner scaling law but with a much larger slip length. For both the superhydrophobic surfaces tested, Petrov and Petrov's combined hydrodynamic-molecular model was found to fit the behavior of the dynamic receding contact angles well over the entire range of capillary numbers observed.

ACKNOWLEDGMENTS

This research was supported by the Center for Hierarchical Manufacturing at University of Massachusetts Amherst under NSF Grant Nos. CMMI-1025020 and CBET-1334962.

[1] W. Barthlott and C. Neinhuis, "Purity of the sacred lotus, or escape from contamination in biological surfaces," Planta **202**, 1 (1997).
[2] E. A. Hebets and R. F. Chapman, "Surviving the flood: Plastron respiration in the non-tracheatearthropod Phrynus marginemaculatus (Amblypygi: Arachnida)," J. Insect Physiol. **46**, 13 (2000).
[3] D. L. Hu, B. Chan, and J. W. M. Bush, "The hydrodynamics of water strider locomotion," Nature **424**, 663 (2003).
[4] T. Nørgaard and M. Dacke, "Fog-basking behaviour and water collection efficiency in Namib Desert Darkling beetles," Front. Zool. **7**, 23 (2010).
[5] N. J. Shirtcliffe, G. McHale, M. I. Newton, C. C. Perry, and F. B. Pyatt, "Plastron properties of a superhydrophobic surface," Appl. Phys. Lett. **89**, 104106 (2006).
[6] N. J. Shirtcliffe, F. B. Pyatt, M. I. Newton, and G. McHale, "A lichen protected by a super-hydrophobic and breathable structure," J. Plant Physiol. **163**, 1193 (2006).

[7] Y. Zheng, X. Gao, and L. Jiang, "Directional adhesion of superhydrophobic butterfly wings," Soft Matter **3**, 178 (2007).
[8] M. Reyssat, A. Pepin, F. Marty, Y. Chen, and D. Quere, "Bouncing transitions on microtextured materials," Europhys. Lett. **74**, 306 (2006).
[9] D. Richard and D. Quere, "Bouncing water drops," Europhys. Lett. **50**, 769 (2000).
[10] M. Nilsson and J. P. Rothstein, "The effect of contact angle hysteresis on droplet coalescence and mixing," J. Colloid Interface Sci. **363**, 646 (2011).
[11] M. Nilsson and J. P. Rothstein, "Using sharp transition in contact angle hysteresis to move and deflect droplets on a superhydrophobic surface," Phys. Fluids **24**, 062001 (2012).
[12] J. P. Rothstein, "Slip on superhydrophobic surfaces," Annu. Rev. Fluid Mech. **42**, 89 (2010).
[13] J. Ou and J. P. Rothstein, "Direct velocity measurements of the flow past drag-reducing ultrahydrophobic surfaces," Phys. Fluids **17**, 103606 (2005).
[14] J. Ou, J. B. Perot, and J. P. Rothstein, "Laminar drag reduction in microchannels using ultrahydrophobic surfaces," Phys. Fluids **16**, 4635 (2004).
[15] R. Daniello, N. E. Waterhouse, and J. P. Rothstein, "Turbulent drag reduction using superhydrophobic surfaces," Phys. Fluids **21**, 085103 (2009).
[16] P. G. de Gennes, F. Brochard-Wyart, and D. Quéré, *Capillarity and Wetting Phenomena: Drops, Bubbles, Pearls, Waves* (Springer, New York, 2004).
[17] J. C. Berg, *Wettability* (Marcel Dekker, Inc., New York, 1993).
[18] R. Hoffman, "A study of the advancing interface. I. Interface shape is liquid-gas systems," J. Colloid Interface Sci. **50**, 228 (1975).
[19] E. B. Dussan, "On the spreading of liquids on solid surfaces: Static and dynamic contact lines," Annu. Rev. Fluid Mech. **11**, 371 (1979).
[20] R. E. Johnson, R. H. Dettre, and D. A. Brandeth, "Dynamic contact angles and contact angle hysteresis," J. Colloid Interface Sci. **62**, 205 (1977).
[21] G. Strom, M. Fredriksson, P. Stenius, and B. Radoev, "Kinetics of steady-state wetting," J. Colloid Interface Sci. **134**, 107 (1990).
[22] T. D. Blake and K. J. Ruschak, "A maximum speed of wetting," Nature **282**, 489 (1979).
[23] R. Burley and R. P. S. Jolly, "Entrainment of air into liquids by a high speed continous solid surface," Chem. Eng. Sci. **39**, 1357 (1984).
[24] J. G. Petrov, J. Ralston, M. Schneemilch, and R. A. Hayes, "Dynamics of partial wetting and dewetting in well-defined systems," J. Phys. Chem. **107**, 1634 (2003).
[25] C. Huh and L. E. Scriven, "Hydrodynamic model of steady movement of a solid/liquid/fluid contact line," J. Colloid Interface Sci. **35**, 85 (1971).
[26] O. V. Voinov, "Hydrodynamics of wetting," Fluid Dyn. **11**, 714 (1976).
[27] L. H. Tanner, "The spreading of silicone oil drop on horizontal surfaces," J. Phys. D: Appl. Phys. **12**, 1473 (1979).
[28] R. G. Cox, "The dynamics of the spreading of liquids on a solid surface. Part 1. Viscous flow," J. Fluid Mech. **168**, 169 (1986).
[29] J. H. Snoeijer and B. Andreotti, "Moving contact lines: Scales, regimes, and dynamical transitions," Annu. Rev. Fluid Mech. **45**, 269 (2013).
[30] J. Eggers and H. A. Stone, "Characteristic lengths at moving contact lines for a perfectly wetting fluid: The influence of speed on the dynamic contact angle," J. Fluid Mech. **505**, 309 (2004).
[31] L. M. Hocking, "Rival contact-angle models and the spreading of drops," J. Fluid Mech. **239**, 671–681 (1992).
[32] J. Eggers, "Existence of receding and advancing contact lines," Phys. Fluids **17**, 082106 (2005).
[33] C. G. Ngan and E. B. Dussan V., "On the nature of the dynamic contact angle: An experimental study," J. Fluid Mech. **118**, 27 (1982).
[34] J. E. Seebergh and J. C. Berg, "Dynamic wetting in the low capillary number regime," Chem. Eng. Sci. **47**, 4455 (1992).
[35] J. H. Snoeijer, "Free-surface flows with large slopes: Beyond lubrication theory," Phys. Fluids **18**, 021701 (2006).
[36] S. F. Kistler, in *Wettability*, edited by J. C. Berg (Marcel Dekker, New York, 1993), p. 311.
[37] M. Bracke, F. De Voeght, and P. Joos, "The kinetics of wetting: The dynamic contact angle," Prog. Colloid Polym. Sci. **79**, 142 (1989).
[38] T. D. Blake and J. M. Haynes, "Kinetics of liquid/liquid displacement," J. Colloid Interface Sci. **30**, 421 (1969).
[39] M. Schneemilch, R. A. Hayes, J. G. Petrov, and J. Ralston, "Dynamic wetting and dewetting of a low-energy surface by pure liquids," Langmuir **14**, 7047 (1998).
[40] T. D. Blake and Y. D. Shikhmurzaev, "Dynamic wetting by liquids of different viscosity," J. Colloid Interface Sci. **253**, 196 (2002).
[41] T. D. Blake, "The physics of moving wetting lines," J. Colloid Interface Sci. **299**, 1 (2006).
[42] M. Nilsson, R. Daniello, and J. P. Rothstein, "A novel and inexpensive technique for creating superhydrophobic surfaces using Teflon and sandpaper," J. Phys. D: Appl. Phys. **43**, 045301 (2010).
[43] P. Muralidhar, N. Ferrer, R. Daniello, and J. P. Rothstein, "Influence of slip on the flow past superhydrophobic circular cylinders," J. Fluid Mech. **680**, 459 (2011).
[44] D. Song, R. Daniello, and J. P. Rothstein, "Drag reduction using superhydrophobic sanded Teflon surfaces," Exp. Fluids **55**, 1783 (2014).
[45] P. Petrov and I. Petrov, "A combined molecular-hydrodynamic approach to wetting kinetics," Langmuir **8**, 1762 (1992).
[46] J. W. Krumpfer and T. J. McCarthy, "Dip-coating crystallization on a superhydrophobic surface: A Million mounted crystals in a 1 cm2 array," J. Am. Chem. Soc. **133**, 5764 (2011).
[47] P. G. de Gennes, "Wetting: Statics and dynamics," Rev. Mod. Phys. **57**, 827 (1985).